Surface Characterization of $CuInS_2$ with Lamellar Morphology

S. Cattarin and C. Pagura

Istituto di Polarografia ed Elettrochimica Preparativa del C. N. R., Corso Stati Uniti 4, 35100 Padova, Italy

L. Armelao and R. Bertoncello

Dipartimento di Chimica Inorganica Metallorganica ed Analitica, via Loredan 4, 35131 Padova, Italy

N. Dietz

Department of Materials Science and Engineering, North Carolina State University, Raleigh, North Carolina 27695, USA

ABSTRACT

Lamellar crystals of $CuInS_2$ grown in a steep temperature gradient have been characterized. Dispersive x-ray analyses show a predominant stoichiometry Cu/In/S = 1/1/2 and inclusions of Cu deficient phases. The cleaved surface is smooth, but after chemical etching a fine structure appears, with a great number of closely packed microcrystals of a dendritic shape. X-ray diffraction spectra of lamellae only show the reflections of the $CuInS_2$ (112) and of the $CuIn_5S_8$ (111) lattice planes, indicating a strongly oriented structure. Depth profiles of $CuInS_2$ lamellae investigated with x-ray photoelectron spectroscopy show the presence at the cleaved surface of Cu deficient phases like $CuIn_5S_8$, which are a few tens of nanometers thick. The lamellar growth mechanism is discussed on the basis of these findings. X-ray photoelectron spectroscopy and secondary ion mass spectrometry investigations show that the oxidation behavior of the lamellar material resembles that of traditional $CuInX_2$ phases (X = S, Se).

Introduction

Efficient thin film solar cells require materials with high optical absorptivity, α, and suitable energy gaps, E_g. The theoretical efficiency is good for E_g ranging between 1 and 2 eV, and it is maximum for $1.1 \leq E_g \leq 1.5$ eV.[1] Due to their properties, the chalcopyrites $CuInX_2$ ($\alpha \cong 10^5$ cm^{-1}, E_g = 1.0 and 1.5 eV for X = S and Se, respectively) are among the few materials with a potential applicability in solar energy conversion. $CuInSe_2$-based thin film cells have already achieved efficiencies up to 15% under simulated AM 1.5 conditions.[2-4] Development of $CuInS_2$, which has a bandgap in the optimum range, has lagged behind for a long time. However, a conversion efficiency exceeding 10% has been recently reported for a polycrystalline p-$CuInS_2$/n-CdS thin film junction under simulated AM 1.5 conditions.[5]

Besides development of the thin film configuration, further investigation of bulk material growth appears justified both to extend the fundamental knowledge and to improve the quality of single-crystalline material for applications in efficient devices using concentrators. An intrinsic problem of $CuInS_2$ growth, as compared with the selenide analogue, is the much larger sulfur vapor pressure, leading to bubble formation within the melt. In trying to eliminate this drawback, crystal growth by the gradient freeze method in the presence of an Ar overpressure was recently explored.[6,7] The stoichiometric melt was cooled by a rate of 1°C/h from 1100°C (at which temperature the Ar pressure was about 25 bar) to 970°C through three transition points,[6] then to room temperature by a rate of 100°C/h. The ingots obtained were essentially bubble-free and showed different morphologies depending on the applied temperature gradient G. Large single crystals were obtained at $G \leq 5°C \cdot cm^{-1}$, while an unexpected lamellar morphology resulted at $G \geq 10°C \cdot cm^{-1}$.[6]

The photoconversion performance of the lamellar material has been investigated in liquid junction with aqueous acidic polyiodide.[8-10] The electrodes show variable photoelectrochemical response, including photoconductivity phenomena, indicating heterogeneous electronic properties.[9] Photoconversion efficiency is generally quite low, but selected samples have shown promising performance, with a solar to electric energy conversion efficiency $\eta \cong 7\%$ under simulated AM 1 conditions.[8]

Structural and defect characterization of $CuInS_2$ grown under Ar overpressure have been the object of previous papers.[6,7] Here we present an investigation of the cleaved surfaces with the aim of characterizing the composition of the thin surface layer which is most important during junction formation and of clarifying the growth mechanism which may be of interest in homogeneous thin layers preparation.[5]

Experimental

Lamellar $CuInS_2$ was prepared with the gradient freeze technique.[6,7,11] Samples were fixed to suitable holders by means of conductive silver epoxy and fresh surfaces were obtained by peeling off crystal layers with adhesive tape. Investigations were performed both on samples peeled and transferred to the analysis chamber under an inert gas (N_2) and on samples previously exposed to oxygen.

Scanning electron microscopy (SEM) investigations were performed with a Philips Model XL 40 LaB_6 apparatus, equipped with a secondary electron detector (SE) and a solid-state detector for back-scattered electrons (BSE). Energy dispersive x-ray (EDX) analyses were performed using an EDAX PV 99 spectrometer equipped with a thin beryllium window. Quantitative measurements were corrected taking into account the factors of atomic number Z, absorption A, and fluorescence F (ZAF correction). An electron beam energy of 25 keV was used, resulting in a sampling depth of about 2.5 μm). X-ray diffractograms were obtained on a Philips PW3710 instrument, using the Cu Kα radiation (40 kV and 30 mA, narrow divergence slit of 1/6 degree).

X-ray photoelectron spectroscopy (XPS) was run on a Perkin Elmer PHI 5600ci spectrometer with nonmonochromatized Mg Kα and Al Kα radiations (1253.6 and 1486.6 eV, respectively). The working pressure was less than 2×10^{-7} Pa. The spectrometer was calibrated by assuming the binding energy (BE) of the Au $4f_{7/2}$ line at 83.9 eV with respect to the Fermi level. The C1s line of adventitious carbon was assumed at 284.8 eV as internal reference for the peak positions.[12] Survey scans (187.85 eV pass energy, 1 eV step, 0.5 s/step dwell time) were obtained in the BE range between 0 and 1200 eV. Detailed scans were recorded at 5.85 eV pass energy, 0.1 eV step, 1.0 s/step dwell time for the In ($3d_{5/2}$ and $3d_{3/2}$ lines), Cu ($2p_{3/2}$ and $2p_{1/2}$ lines), S ($2p_{3/2+1/2}$ line), O1s and C1s lines, together with the corresponding Auger lines for In and Cu. The chemical states of the various elements were in agreement with literature data.[13,14] The standard deviation in the BE values of the XPS lines was 0.1 eV. After a Shirley-type background subtraction,[15] the raw spectra were fitted using a nonlinear least square fitting program adopting Gaussian-Lorentzian peak shapes for all peaks.[16] The atomic compositions were

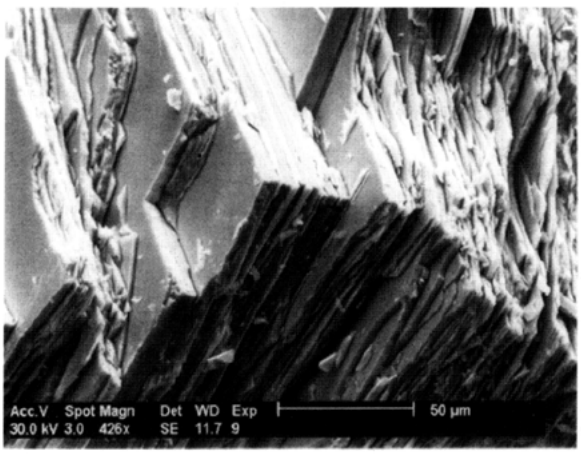

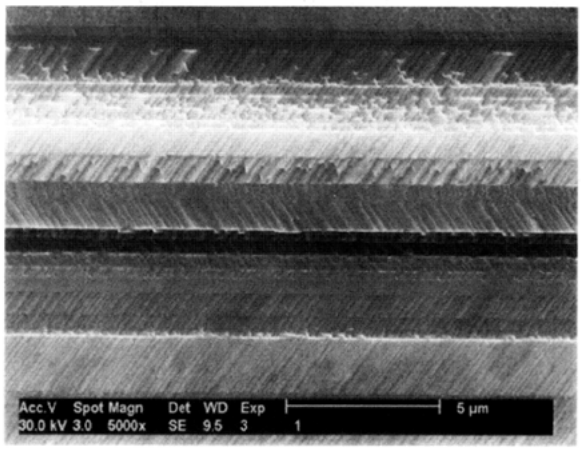

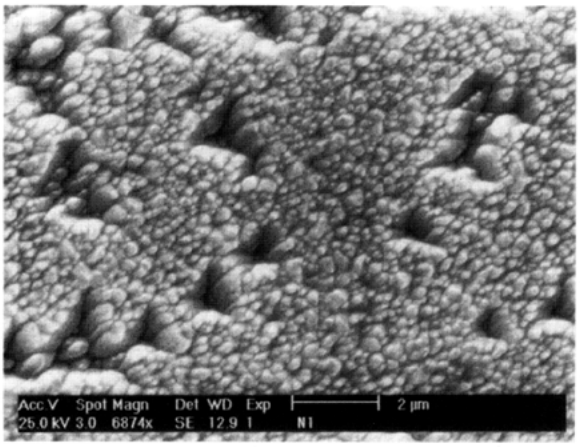

Fig. 1. SEM micrographs showing: (a, top left) lamellar morphology of crystals; (b, above) crystal section made perpendicular to cleavage plane showing fine, dendritic structure of lamellae; (c, left) aspect of cleavage plane after corrosion/photocorrosion in polyiodide medium.

evaluated using sensitivity factors as determined from theoretical photoionization cross sections and asymmetry parameters calculated within the Hartree-Fock-Slater one-electron central potential model.[17]

The XPS spectra were recorded at a takeoff angle of 45°. Angle-resolved (ARXPS) investigations were performed comparing the spectra recorded at takeoff angles varying between 10° and 90°. The analysis chamber was equipped with a scanning electron microscopy/scanning Auger microscopy instrument, which was used in some cases for inspection of the area sampled by XPS technique. Depth profiles were carried out by Ar^+ sputtering at 2.5 keV, 400 nA cm^{-2} beam current density with an argon partial pressure of 5×10^{-6} Pa. The beam voltage and current were chosen to minimize preferential sputtering.[18] Under these conditions we estimated a sputtering rate in the order of 3 nm min^{-1}. A bulk $CuInS_2$ crystal was analyzed before and after Ar^+ etching for comparison. The quantitative analysis of the as-cleaved crystal surface was in agreement with nominal stoichiometry. After Ar^+ sputtering S deficient stoichiometries $CuInS_x$ were observed ($x = 1.8 \pm 0.1$), indicating sulfur preferential sputtering.

SIMS spectra were taken on a custom-built instrument,[19,20] based on a quadrupole mass analyzer. The samples were exposed to a rastered (2 × 2 mm), 3 keV, 650 nA Ar^+ ion beam.

Results

Lamellar morphology and crystal structure.—The material has a peculiar lamellar aspect (Fig. 1a). The bulk of the lamellae is polycrystalline as suggested by spectroscopy[7] and confirmed by SEM micrographs (Fig. 1). The cleavage surface, originally smooth to SEM inspection, shows after corrosion in acidic polyiodide[9] a great number of closely packed microcrystals (Fig. 1c). The side view provided by a section of the lamellar crystal (Fig. 1b) indicates that the "bulk" of each lamella consists of a number of microcrystals, filamentous or dendritic in aspect, with a morphology also observed in thin films.[21] The dendrites form an angle of 55° with the cleavage plane, corresponding to the angle between (112) plane and [110] direction in the chalcopyrite structure. Hence, the crystal is highly oriented despite its heterogeneity.

The XRD spectrum of powders (Fig. 2b) is that typical for a single-phase chalcopyrite $CuInS_2$, as reported in JCPDS data files (Fig. 2a). Conversely, the spectrum of a lamellar crystal (Fig. 2c) only shows two major peaks at $2\theta \cong 27.9°$ and $2\theta \cong 57.6°$, corresponding to (112) and (224) planes, respectively. This finding confirms a strong crystal orientation and was originally attributed to the presence of extended monocrystalline regions cleaving along (112) planes.[6,7] Besides the dominant peaks of the chalcopyrite $CuInS_2$ phase (ch), Fig. 2c shows the reflections of the (111) lattice planes of the spinel $CuIn_5S_8$ phase (sp).

SEM micrographs of the cleavage surface taken with a BSE detector show regions of different brightness (Fig. 3, top). Whereas the predominant EDX stoichiometry is Cu/In/S = 1/1/2, in the brighter areas the material shows ratios Cu/In < 1, henceforth frequently referred to as Cu deficient, with Cu contents down to 7 to 8 atom percent (a/o). A variety of Cu/In/S stoichiometries between 1/1/2 and 1/5/8 is observed in the bright SEM regions, the figure 1/3/5 being the most common.[10] Whereas there is no final evidence in the literature of a distinct $CuIn_3S_5$ phase (see Ref. 10 and references therein), the spinel phase $CuIn_5S_8$ is well known.[22] The variability of EDX data can be attributed to the presence of Cu deficient phases thinner than the sampling depth of the technique, so that EDX apparent stoichiometries may include contributions from the $CuInS_2$ host phase. Cu deficient phases are seldom observed in sections like that of Fig. 1b, and are more common on the surfaces obtained by peeling off the crystal sheets, suggest-

ing that the crystal cleaves preferentially in correspondence of these foreign phases.

Surface composition of the as-cleaved crystal.—Angle-Resolved XPS analysis.—XPS investigations are performed on freshly peeled samples, transferred to the analysis chamber avoiding contact with air. After analysis, the samples are inspected by EDX to check the presence of Cu deficient phases, and only the XPS data relevant to samples with quite homogeneous "bulk" $CuInS_2$ composition are discussed in this section. XP spectra (not reported) show the peaks of Cu, In, and S elements at binding energies typical of chalcopyrites[23-27]: In $3d_{5/2}$ line at 444.8 eV, Cu $2_{p3/2}$ line at 932.5 eV, and S $2p_{3/2}$ line at 161.8 eV. The oxygen peak is negligible. A typical surface stoichiometry Cu/In/S estimated from XP spectrum is $1/3.6 \pm 0.2/6.0 \pm 0.4$. Considering only ternary phases along the pseudobinary line Cu_2S-In_2S_3, this stoichiometry may represent the average of contributions from thin surface layers of $CuIn_5S_8$ (and possibly $CuIn_3S_5$), and the host phase $CuInS_2$.

ARXPS experiments show a significant dependence of composition on detection angle, with the same qualitative trend in three examined samples. Some variation in the values and a nonmonotonous dependency of the composition on the sampling angle are observed, which may be accounted for by a nonhomogeneous surface stoichiometry, confirmed by XPS line scan experiments. The Cu content (7 to 9 a/o) and the ratio Cu/In ≅ 1/5 are minimum for grazing takeoff angles, corresponding to minimum sampling depths (≤1.8 nm for Cu 2p line). On increasing the takeoff angle the Cu content gradually increases and so does the Cu/In ratio. For perpendicular detection (sampling depth ≤5.4 nm for Cu 2p line) a Cu content of 11 to 13 a/o and a ratio Cu/In ≅ 1/2.5 or 1/3 are observed. These data show segregation of a phase with lower Cu content in the outermost layers close to the "fracture surfaces" exposed after cleaving. Considering only stoichiometries corresponding to the pseudobinary line Cu_2S-In_2S_3, the outermost layer composition approaches that of the spinel phase $CuIn_5S_8$.

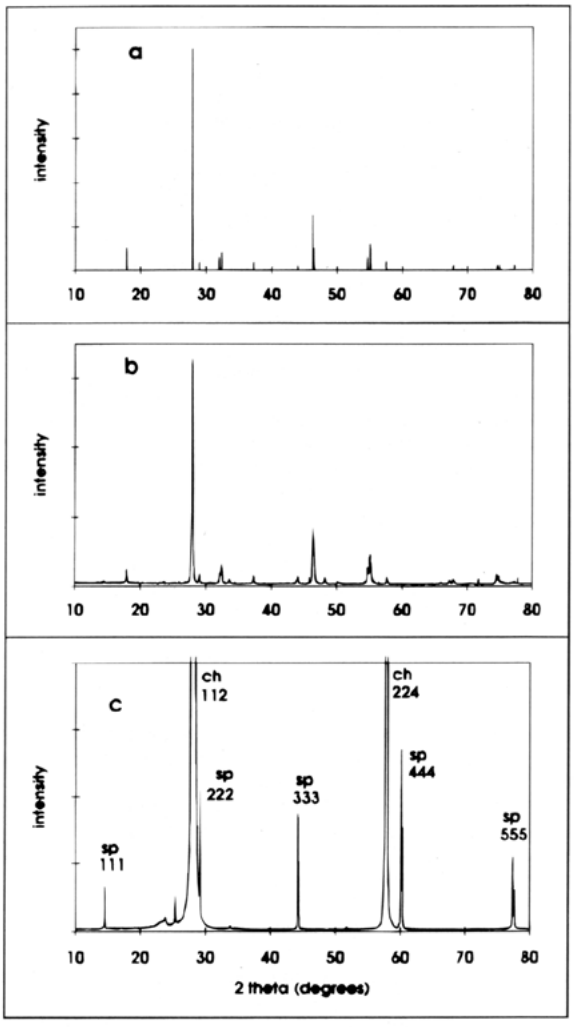

Fig. 2. X-ray diffractograms (Cu Kα radiation λ = 1.5406 Å): (a) reference file data for chalcopyrite (ch) $CuInS_2$ (JCPDS 27-159); (b) spectrum of powders of lamellar $CuInS_2$; (c) spectrum of a lamellar $CuInS_2$ crystal showing the main chalcopyrite (ch) peaks for (112) and (224) planes and peaks of the spinel phase (sp) $CuIn_5S_8$ (JCPDS 24-361).

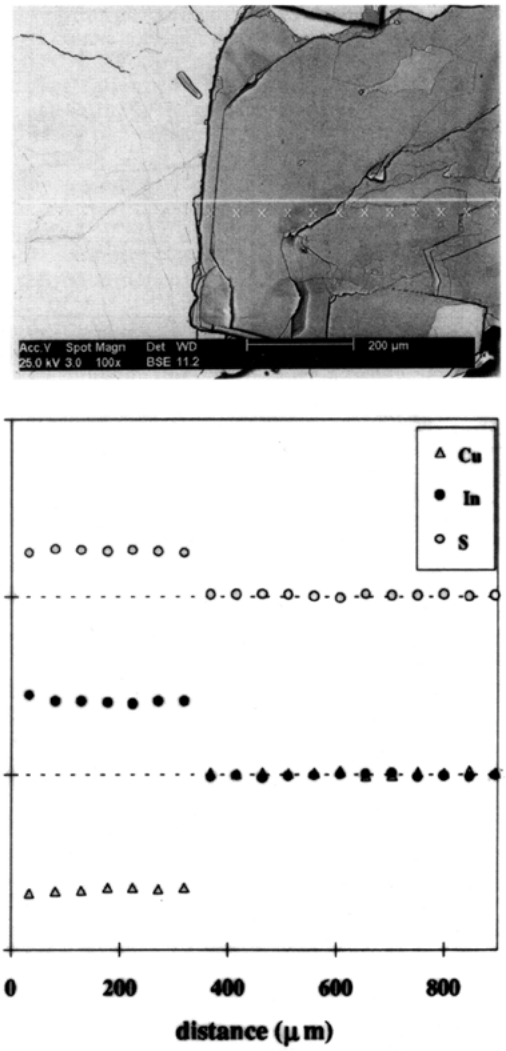

Fig. 3. SEM micrograph (top) of a heterogeneous region of the lamellar material and relevant EDX microanalysis (bottom). The atomic ratios Cu/In/S are about 1/1/2 in the dark area and 1/3.9/6.2 in the bright area.

Depth profile of the lamellae.—Surface analysis and depth profiles are performed in the two regions of the sample of Fig. 3 with different EDX composition. Accurate sample positioning is made possible by the SEM instrument in the analysis chamber, providing unequivocal identification of the regions with different composition on the basis of surface morphology. Exposure to air of the sample prior to XPS analysis cannot be avoided. However, XP spectra (Fig. 4) show a very small oxygen signal. The C and O peaks become negligible after the first sputtering cycle and the relevant signals are not reported in the depth pro-

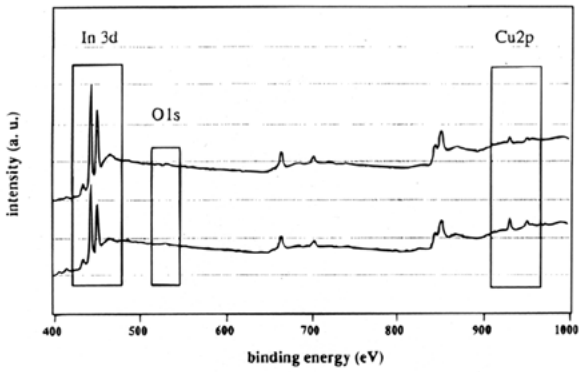

Fig. 4. XP spectra taken on the same crystal of Fig. 3 in the two regions with Cu deficient EDX stoichiometry (top) and with stoichiometry of the $CuInS_2$ phase (bottom).

files of Fig. 5 and 6, which may be considered representative of the pristine unoxidized material.

The XP spectrum taken in the area of Fig. 3 with EDX composition Cu/In/S close to 1/1/2 is shown in Fig. 4, bottom. The oxygen signal represents a few a/o and the Cu/In/S atomic ratios are very similar to those recorded at the unoxidized samples, discussed in the previous section. Figure 5 shows the XPS depth profile. The copper content and the Cu/In ratio rapidly increase after the first sputtering cycles, up to 10 min of sputtering corresponding to an estimated depth of 30 nm, where Cu/In ≅ 1/1.2. Peak shapes and positions do not vary significantly after sputtering treatment. Proceeding in the depth profile, the Cu content increases further more slowly, and the Cu/In ratio attains the value of 1 by the estimated depth of 60 nm. In the latter condition, taking into account effects of sulfur loss discussed in the Experimental section, the XP analysis corresponds to the "bulk" EDX composition. Scanning Auger analysis of the area sampled by XPS (about 400 × 400 μm) before and after sputtering does not show local accumulations of elements resulting from the ion etching treatment, within the instrumental resolution of about 200 nm.

The XP spectrum taken in the area of Fig. 3 with EDX composition Cu/In/S ≅ 1/3.9/6.2 is shown in Fig. 4, top. The surface stoichiometry evaluated from XP spectrum is about 1/10/13, with a Cu/In ratio not far from that of the $CuIn_{11}S_{17}$ phase.[28,29] Considering only compositions along the binary line Cu_2S-In_2S_3, the S content appears significantly below stoichiometric equivalence with the metals.

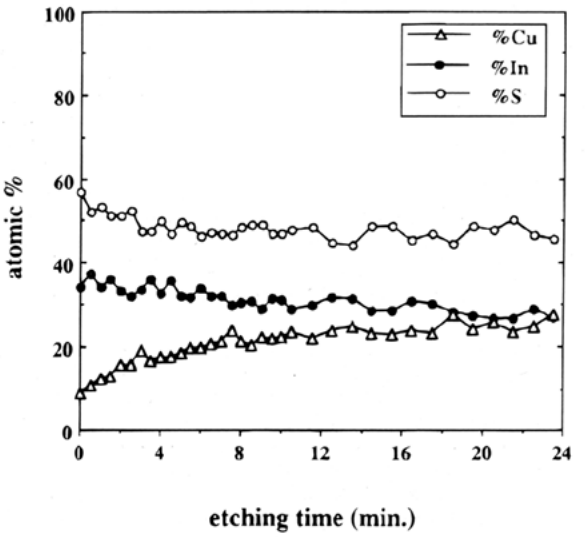

Fig. 5. XPS depth profile taken on the same crystal of Fig. 3 in the region with EDX composition Cu/In/S ≅ 1/1/2.

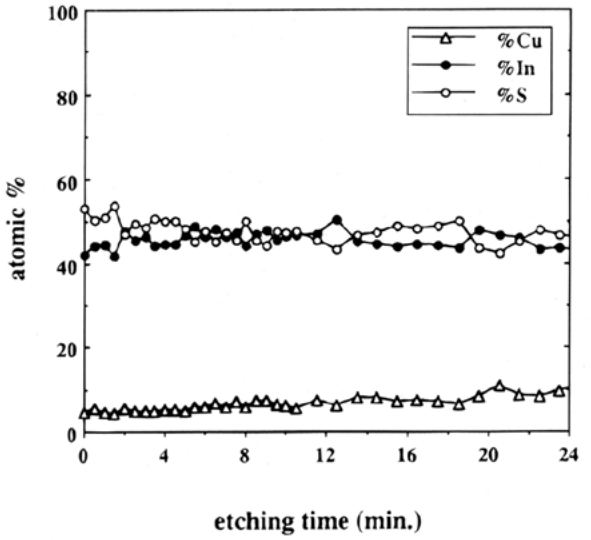

Fig. 6. XPS depth profile taken on the same crystal of Fig. 3 in the region with Cu deficient EDX composition Cu/In/S ≅ 1/3.9/6.2.

Inclusion of In-S phases like InS or In_6S_7 [30] would better account for the observed stoichiometry; however, In_2S_3 and InS cannot be distinguished by their XP spectra (see Ref. 31 and references therein), and this point could not be assessed further. Figure 6 shows the XPS depth profile recorded by sputtering this area. Even in this case the surface region is Cu depleted as compared to the bulk and the Cu content increases going deeper, but the variation is more gradual than that observed in Fig. 5. The Cu/In ratio, close to 1/10 at the surface, approaches 1/5 after removal of about 60 to 70 nm of material. Assuming that some sulfur preferential sputtering occurs also in this case, the "bulk" composition approaches that of $CuIn_5S_8$.

Surface oxidation in the air.—The XP spectra of the lamellar material exposed to air for a few days, at room temperature, show limited changes as compared to the spectra of the pristine material. No appreciable shift is observed in the positions of In and Cu lines. The absence of the Cu shake-up lines ensures that no significant amount of Cu(II) forms.[13,14] The position and shape of the S lines is unaltered within experimental accuracy and no significant signal arises in the region typical of oxidized sulfur species like sulfate. A small O 1s peak is present, located at a binding energy of 531.8 eV, in a position typical of hydroxides. Since Cu(I) hydroxide is unstable and rapidly converts to Cu_2O, whose O 1s peak occurs at 530.3 eV, [13] the observed O peak position only fits literature values for $In(OH)_3$. [13] The presence of $In(OH)_3$ is compatible with the observation of no energy shifts in the In lines.[13] XPS depth profiles indicate that exposure to atmospheric oxygen causes oxidation of a very thin surface layer. The XPS oxygen peak typically represents 10 to 20 a/o at the surface and disappears after 60 to 90 s sputtering (3 to 4.5 nm of material).

To better characterize the chemical bindings of the surface species we have also run SIMS spectra on an oxidized surface showing EDX composition close to $CuInS_2$. In the spectrum (Fig. 7), several peaks attributable to fragments containing the original atoms Cu, In, and S are observed. No significant peak can be accounted for by fragments containing both O and Cu, whereas at least three peaks correspond to fragments containing both O and In. The rapid decrease in time of the signal relevant to the ion with mass unit 246 (In_2O^+) confirms XPS indications of formation of a thin oxidized layer.

SIMS and XPS data show that surface oxidation in the air proceeds with the formation of a thin passivating layer, a few nanometers thick, containing $In(OH)_3$ or related oxides and copper chalcogenides Cu_2S or CuS, in which Cu is present as Cu(I). [32] These findings resemble those reported

for the oxidation of single crystals and polycrystalline $CuInS_2$ [23] or $CuInSe_2$ [26,27,33] in which the oxidation products had been identified as Cu_yX (X = S, Se) and $In(OH)_3$.

Discussion and Conclusions

The crystal bulk of lamellar $CuInS_2$ consists of closely packed, highly oriented, dendritic microcrystals. The lamellar morphology originates from a periodic interruption of their growth over a front that is very large in comparison with the section of a single dendrite. ARXPS and XPS depth profiles show segregation at the lamella surface of Cu depleted phase(s), with a prevailing stoichiometry close to that of the $CuIn_5S_8$ spinel phase, and a thickness estimated in the range of a few tens of nanometers. The presence of the $CuIn_5S_8$ phase is also confirmed by XRD evidence. Besides the predominant $CuInS_2$ phase, the material contains lamellar regions in which the EDX Cu/In/S atomic ratios are in the range between 1/3/5 and 1/5/8. Cu depletion at the surface (as compared to the bulk) is also observed in the latter regions.

The presence of a Cu deficient (spinel) phase in between the lamellae of chalcopyrite structure may explain the cleaving behavior. The {111} spinel face may epitaxially grow over the {112} face of the $CuInS_2$ matrix, but due to lattice mismatch strain is present.[11] The easy crystal cleaving in correspondence of the foreign phase results in the lamellar morphology.

The presence of a steep temperature gradient during crystal growth is essential to the appearence of the the heavy twinned structure and the lamellar morphology.[6,7] A tentative mechanism accounting for the periodic formation of a Cu deficient phase may be proposed assuming that in the given conditions the $CuInS_2$ solid forms with a slight Cu_2S excess. Hence, the melt in contact with the solid is more and more depleted of the corresponding elements, until a critical composition is reached causing the crystallization of distinct Cu deficient phases like $CuIn_5S_8$ and, possibly, $CuIn_3S_5$. This causes recovery of a nearly stoichiometric melt composition and epitaxial growth of solid $CuInS_2$ starts again. The exact mechanism which allows this highly oriented growth of at least two phases is not fully understood at present and needs further investigations, assessing details of the growth process such as the excursions in the liquidus composition at the solid-liquid interface.

However, recent literature reports may indicate that the phenomena are not peculiar to the gradient freeze method. Formation of Cu deficient phases is even observed on top of

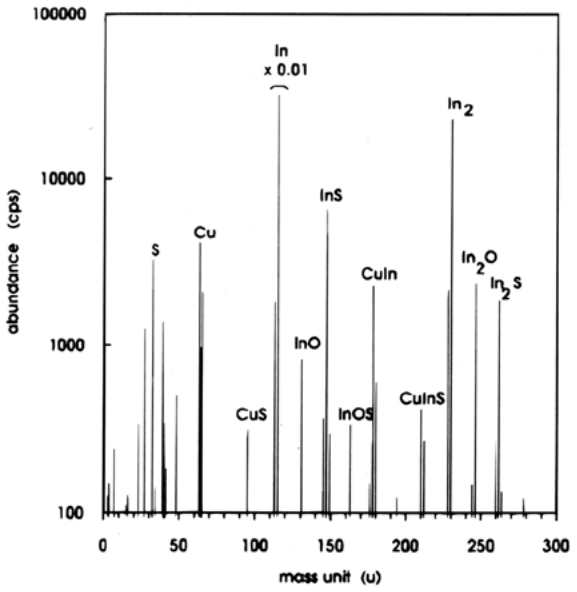

Fig. 7. Positive ion mass spectra of the surface of a lamellar $CuInS_2$ sample exposed to air for a week.

$CuInS_2$ thin films prepared in an ultrahigh vacuum system by thermal co-evaporation of the elements on a substrate kept at 500°C. [24,25] For bulk cation ratios $(Cu/In)_{bulk}$ close to 1, the surface cation ratio is $(Cu/In)_{surface} \cong 1/3$, [24] and the presence of a $CuIn_3X_5$ phase has been proposed.[34] The presence of a large temperature gradient in the conditions of film synthesis appears very likely, but it is not known whether the analogies with the lamellar material are a clue to a common growth mechanism.

The reported SEM, EDX, XPS characterizations show significant variability in the composition of lamellar $CuInS_2$, reflecting nonequilibrium growth conditions and complexity of the Cu-In-S phase diagram.[30] Given the critical importance of stoichiometry in defining the electronic properties of ternary chalcopyrite semiconductors,[35,36] this fact may account for the heterogeneous behavior of photoelectrodes,[9] including presence of both n- and p-type conductivities, and for their low average performances. However, the observation of promising performance at selected samples[8] calls for an additional effort in material synthesis. Investigations of lamellar crystal growth are currently in progress[11] with the aim of preparing more homogeneous material and of clarifying the open questions on the growth mechanism.

Acknowledgments

The authors are grateful to Dr. P. Guerriero (ICTIMA-CNR, Corso Stati Uniti 4, Padova) for SEM-EDX investigations, to Dr. U. Casellato (ICTIMA-CNR) for XRD spectra, to B. Facchin (IPELP-CNR, Corso Stati Uniti 4, Padova) for running the SIMS spectra. The XPS analyses were supported by "Progetto Finalizzato Materiali Speciali per Tecnologie Avanzate" of Consiglio Nazionale delle Ricerche, Rome. The authors are especially grateful to Professor H.-J. Lewerenz (Hahn-Meitner-Institut, Berlin) for useful discussions and criticism.

Manuscript submitted Oct. 31, 1994; revised manuscript received April 19, 1995.

Universitá Degli Studi di Padova assisted in meeting the publication costs of this article.

REFERENCES

1. J. J. Loferski, *J. Appl. Phys.*, **27,** 777 (1956); W. Shockley and H. J. Queisser, *ibid.*, **32,** 510 (1961).
2. S. Menezes, H.-J. Lewerenz, and K. J. Bachmann, *Nature,* **305,** 615 (1983).
3. K. Mitchell, C. Eberspacher, J. Ermer, and D. Pier, in *Proceedings 20th IEEE Photovoltaic Specialists' Conference,* p. 1384, Las Vegas, NV, IEEE, New York (1988).
4. L. Stolt, J. HedstrHm, J. Kessler, M. Ruckh, K.-O. Velthaus, and H. W. Schock, *Appl. Phys. Lett.,* **62,** 597 (1993).
5. R. Scheer, T. Walther, H. W. Schock, M. L. Fearheiley, and H. J. Lewerenz, *ibid.,* **63,** 3294 (1993).
6. M. L. Fearheiley, N. Dietz, and H. J. Lewerenz, *This Journal,* **139,** 512 (1992).
7. N. Dietz, M. L. Fearheiley, S. Schroetter, and H. J. Lewerenz, *Mater. Sci. Eng.,* **B14,** 101 (1992).
8. S. Cattarin, N. Dietz, and H. J. Lewerenz, *This Journal,* **141,** 1095 (1994).
9. S. Cattarin, P. Guerriero, G. Razzini, and H. J. Lewerenz, *ibid.,* **141,** 1100 (1994).
10. S. Cattarin, P. Guerriero, N. Dietz, and H. J. Lewerenz, *Electrochim. Acta,* In press.
11. S. Fiechter *et al.,* In preparation.
12. M. P. Seah and G. C. Smith, in *Practical Surface Analysis,* Vol. 1, 2nd ed., D. Briggs and M. P. Seah, Editors, Appendix 1, pp. 543-544, John Wiley & Sons, Ltd., Chichester, UK (1990).
13. J. F. Moulder, W. F. Stickle, P. E. Sobol, and K. D. Bomben, in *Handbook of X-Ray Photoelectron Spectroscopy,* J. Chastain, Editor, Perkin Elmer Corp., Eden Prairie, MN (1992).
14. *X-Ray Photoelectron Spectroscopy Database,* Version 1.0, National Institute of Standards and Technology, Gaithersburg, MD (1989).
15. D. A. Shirley, *Phys. Rev.,* **55,** 4709 (1972).
16. J. Vegh, *J. Electron Spectr. Rel. Phenom.,* **46,** 411 (1988).

17. J. J. Yeh and I. Lindau, *Atomic Data and Nuclear Data Tables,* **32,** 1 (1985).
18. N. Matsunami, Y. Yamamura, Y. Itikawa, N. Itoh, Y. Kazumata, S. Miyagawa, K. Morita, R. Shimizu, and H. Tawara, *ibid.,* **31,** 1 (1984).
19. C. Pagura, S. Daolio, and B. Facchin, in *Secondary Ion Mass Spectrometry SIMS VIII,* A. Benninghoven, K. T. F. Janssen, J. Tümpner, and H. W. Werner, Editors, pp. 239-242, John Wiley & Sons, Chichester, UK (1992).
20. S. Daolio, B. Facchin, C. Pagura, A. De Battisti, and A. Barbieri, *Rapid Commun. Mass Spectrom.,* **7,** 887 (1993).
21. H. J. Hovel, in *Semiconductors and Semimetals,* Vol. 11 of *Solar Cells,* Chap. 5, Academic Press, Inc., New York (1975).
22. G. Dagan, S. Endo, G. Hodes, G. Sawatzky, and D. Cahen, *Solar Energy Materials,* **11,** 57 (1984).
23. Y. Mirovsky, R. Tenne, D. Cahen, G. Sawatzky, and M. Polak, *This Journal,* **132,** 1070 (1985).
24. R. Scheer and H. J. Lewerenz, *J. Vac. Sci. Technol.,* **A12,** 51 (1994).
25. R. Scheer and H. J. Lewerenz, *ibid.,* **A12,** 56 (1994).
26. L. L. Kazmersky, O. Jamjoum, P. J. Ireland, S. K. Deb, R. A. Mickelsen, and W. Chen, *J. Vac. Sci. Technol.,* **19,** 467 (1981).
27. L. L. Kazmersky, P. J. Ireland, O. Jamjoum, and A. H. Clark, *Scanning Electron Microscopy,* **1,** 285 (1981).
28. H. Minoura, Y. Ueno, H. Kaigawa, and T. Sugiura, *This Journal,* **136,** 1392 (1989).
29. K. Basavaswaran, Y. Ueno, T. Sugiura, and H. Minoura, *J. Mater. Sci.,* **25,** 3456 (1990).
30. H. Migge, *ibid.,* **6,** 2381 (1991).
31. L. L. Kazmersky, P. J. Ireland, P. Sheldon, T. L. Chu, S. S. Chu, and C. L. Lin, *J. Vac. Sci. Technol.,* **17,** 1061 (1980).
32. J. C. W. Folmer and F. Jellinek, *J. Less-Common Met.,* **76,** 153 (1980).
33. L. L. Kazmersky, O. Jamjoum, J. F. Wagner, P. J. Ireland, and K. J. Bachmann, *J. Vac. Sci. Technol.,* **A1,** 668 (1983).
34. D. Schmid, M. Ruckh, F. Grunwald, and H. W. Schock, *J. Appl. Phys.,* **73,** 2902 (1993).
35. J. J. Lofersky, *Mater. Sci. Eng.,* **B13,** 271 (1992).
36. H.Y. Ueng and H.L. Hwang, *J. Appl. Phys.,* **62,** 434 (1987).

Reprinted from JOURNAL OF THE ELECTROCHEMICAL SOCIETY
Vol. 142, No. 8, August 1995
Printed in U.S.A.